J Mater Sci (2007) 42:1733–1750
DOI 10.1007/s10853-006-0906-x

Plastic anisotropy in aluminum and copper pre-strained by equal channel angular extrusion

Irene J. Beyerlein · David J. Alexander · Carlos N. Tomé

Received: 31 May 2006 / Accepted: 31 August 2006 / Published online: 9 January 2007

Abstract The mechanical response of as-processed equal channel angular extrusion materials is anisotropic, depending on both direction and sense of straining. The stress–strain curves exhibit hardening characteristics different from the usual work hardening responses, e.g., Stages I–IV, expected in annealed fcc metals under monotonic loading. In this work, the anisotropic flow responses of two pure fcc metals, Al and Cu, processed by route Bc are evaluated and compared based on pre-strain level (number of passes), direction of reloading, sense of straining (i.e., compression versus tension), and their propensity to generate subgrain microstructures and to rearrange, should the slip activity change. In most cases, either macroscopic work softening or strain intervals with little to no work hardening are observed. Application of a crystallographically based single-crystal hardening law for strain-path changes [Beyerlein and Tomé, Int. J. Plasticity (2007)] incorporated into a visco-plastic self-consistent (VPSC) model supports the hypothesis that suppression of work hardening is due to reversal or cross effects operating at the grain level.

I. J. Beyerlein (✉)
Theoretical Division, Los Alamos National Laboratory,
Los Alamos, NM 87545, USA
e-mail: irene@lanl.gov

D. J. Alexander · C. N. Tomé
Materials Science and Technology Division,
Los Alamos National Laboratory,
Los Alamos, NM 87545, USA

Introduction

The equal channel angular extrusion (ECAE) forming process [1] is characterized by large non-monotonic deformation histories. It involves extruding a metal through a die formed by two channels with equal cross sections intersecting at an angle Φ (see Fig. 1 where $\Phi = 90°$). Each extrusion imposes severe plastic deformation, roughly 80% to 100% strain depending on Φ. Because there is no change in cross section, the sample can be re-inserted repeatedly. Re-insertion unavoidably imposes a strain-path change. Different ECAE routes involve optional rotations about the sample long axis between passes, which alter the sequence and the nature of the strain-path changes. For instance, route Bc prescribes a 90° rotation after every pass and route C, 180°. Through this complex series of severe plastic deformation and strain-path changes, ECAE has proven capable of producing unique, ultra-fine grained microstructures in what was originally a traditional coarse-grained metal [e.g., 2]. In some cases, the final ECAE metal is found to exhibit unusual and desirable mechanical properties (e.g., low temperature superplasticity [3], high strength).

What is often overlooked is that the mechanical properties of ECAE metals will be anisotropic, meaning that they depend on the direction or sense of straining. The deformation anisotropy in flow stress and uniform straining impacts subsequent processing and shaping operations. Only a handful of studies to date have experimentally evaluated the anisotropy of ECAE materials by testing in more than one direction. In all cases, ECAE-processed Ti [4, 5], Al [6], and Cu [7–9] exhibited anisotropic responses. In [8], Cu samples extruded up to four passes with either route Bc or

route C were compressed in one of three directions: parallel to the extrusion direction (ED), parallel to the entry channel (ND), or normal to the plane of the die (TD). Regardless of route and pass number, anisotropy in the compression strength in the three directions was present and the out-of-plane response (TD) was higher than the in-plane responses (ND and ED). Similar trends in the tensile yield and ultimate strength of pure Cu extruded under various routes and after several passes were reported in Haouaoui et al. [9]. In fact both the compression and tensile yield stresses of a first-pass Cu sample in [9] followed the same order as those in [8], i.e., TD > ND > ED. Likewise, Ti was found to be stronger when compressed [5] or tensioned [4] normal to the plane of the die (TD) than when tested in-plane. In contrast, after six passes of route Bc, the tensile strength of Al was highest along the ED and intermediate normal to the plane of the die (TD) [6]. For Ti, a hexagonal material, the observed anisotropy may come as no surprise by virtue of its low symmetry crystal structure. Ti is known to utilize multiple slip and twinning modes in deformation, in which their relative activities depend on straining direction. Al and Cu, on the other hand, utilize only one slip mode and are generally believed to harden isotropically.

Mechanical testing of processed ECAE samples imposes a strain-path change. In cubic materials the anisotropy observed is mostly due to strain-path-change effects, rather than to texture. The subsequent flow responses contained transient behaviors characteristic of the type of strain-path change. These include initial jumps, reductions, or multiple inflection points within the first 10% of reloading. Such transients cannot be completely explained by conventional hardening laws developed to represent the usual work hardening Stages I–IV observed under monotonic loading [10] for metals deforming by slip. Explanations lie in the interactions between texture, substructure development, and dislocation mechanics. This work fills a gap that is missing in most models and mechanical test studies.

Due to the severe plastic deformation, ECAE results in substantial texture and microstructural changes to the sample, rendering the material anisotropic. Even after a single pass a well-defined shear texture is formed and the grains become severely elongated in the plane of the die and strongly inclined (e.g., ~20°–30° above the extrusion axis for $\Phi = 90°$) [9, 11, 12]. Most importantly, deformation microstructures develop, subdividing the grain with subgrain boundaries. Larger-scale substructure consists of shear and deformation bands [13, 14], which are on the order of 10 to 10^2 μm apart. The lower scale, inspiring many more experimental evaluations, consists of finer dislocation structures organized into cellular or long planar walls, approximately 1–0.1 μm apart [e.g., 13, 15–17]. These substructures become more distinct and increase in misorientation with number of passes.

In this work, we evaluate and compare the plastic anisotropy of Al and Cu samples processed by route Bc, using the same die (Fig. 1). Particular attention is paid to the transients in the hardening behavior and their relation to material, pass number, and direction of straining. A single-crystal model developed for arbitrary strain-path changes [18] is applied to one-pass samples to understand the influence of material properties on anisotropy. This model has a crystallographically based formulation that can recognize changes in slip activity and relate them to hardening in each slip plane of each grain.

Experimental procedure

The copper was commercially procured oxygen-free electronic grade C10100 rod nominally 9.5 mm in diameter, in the H80 fully drawn condition. Portions of the rod approximately 100 mm in length were annealed for 1 h at 500 °C in an atmosphere of Ar-6 H gas. This produced an equi-axed grain size of about 90 μm.

The 99.99% aluminum material was also commercially procured in the form of rods 9.5 mm in diameter. The rods were annealed in air for 1 h at 350 °C. This produced a grain size that was about 120 μm in the plane perpendicular to the rod axis. The grains were slightly elongated along the length of the rod, with an aspect ratio of about two.

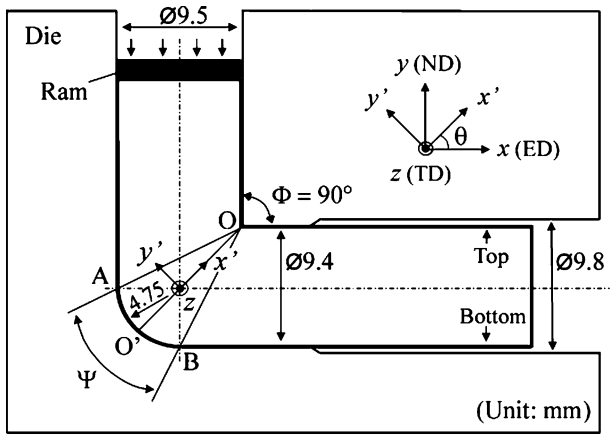

Fig. 1 The ECAE tooling used to process the Al and Cu studied in this work. This figure is taken from [57]

Figure 1 shows the ECAE tooling used to process the Al and Cu. It was fabricated from H13 tool steel, heat-treated to R_C 52. The die angle Φ is 90° and the outer corner radius at the intersection of the inlet and outlet channels was half the inlet channel diameter ($\Psi \sim 37°$). The inlet channel was 9.53 mm in diameter, and the outlet channel was slightly smaller, 9.35 mm in diameter. The outlet channel had a land that extended 5.1 mm from the inner corner and then expanded to 9.80 mm in diameter to reduce the area over which friction acted. The Cu and Al billets were 9.5 mm in diameter and approximately 70 mm in length. The billets and tooling were lubricated with a MoS_2-containing grease. The billets were extruded at room temperature at a ram speed of 2.5 mm/s. Route Bc (90° clockwise rotation of the billet between each pass) was used with the same end of the billet being inserted first into the die for all passes. Successive billets were used to force the final portion of the previous billet around the die corner and out of the die. The surfaces of the extruded billets were clean and shiny, indicating that the MoS_2 lubricant worked effectively. After each extrusion, a small bulge of material was noted on the top surface of the billet immediately behind the billet nose; this bulge was removed by abrasive grinding. The pressing loads increased as the number of passes increased.

Compression cubes 5.08 mm × 5.72 mm × 6.35 mm were sectioned from the billets by electro-discharge machining and compressed in one of three directions along the transverse direction (TD), normal direction (ND), or ED, as indicated in Fig. 1. The compression specimens were tested between polished WC platens, with MoS_2-containing grease to minimize friction. The testing machine crosshead speed was constant, and was selected so that the initial strain rate was 0.001 s^{-1}. For Al, each test was repeated twice. The load–displacement data from the compression tests were converted to engineering stress–strain curves by applying a compliance correction that forced the initial linear portion of the data to fit the known elastic moduli of Cu and Al at room temperature [19] (117 GPa and 62 GPa, respectively). The engineering stress–strain data were then converted to true stress–true strain data assuming uniform deformation of the specimen, even for cases of decreasing load with increasing displacement. For tensile deformation, such a decrease in load generally indicates localized deformation, which make the direct conversion from engineering stress–strain to true stress–strain invalid. In our case, in compression, the deformation remained uniform. Unfortunately due to the small specimen sizes, strain gages could not be placed directly on the sample.

The one-pass Al was also tested in tension in the three orthogonal directions and compared with the one-pass Al compression results as a preliminary investigation into tension–compression asymmetry in ECAE materials. Because of the limit imposed by the billet diameter, very small tensile specimens were machined to measure the tensile properties in the three orthogonal directions defined by the extrusion die. Miniature tensile specimens (gage section 1.27 mm × 1.27 mm × 2.54 mm) were sectioned from the billet by electro-discharge machining, oriented in the three orthogonal directions that matched the die geometry. The tensile specimens were tested on a electromechanical testing machine at a constant crosshead speed of 0.0025 mm/s, for an initial strain rate of 0.001 1/s. For each direction, two specimens were tested. Unlike the compression curves, the tensile curves were cut-off at strain levels where the softening associated with localized deformation begins.

Experimental results

Compression reload results

Figure 2a–c shows, respectively, the compression stress–strain response of pure Al after one to four passes in each of the three directions, TD, ND, and ED. (The results were repeatable, so for some directions, we only show one curve so as to not clutter the plot.) In all straining directions, the material does not strengthen beyond two or three passes. In the TD and ED, the entire flow response of the three- and four-pass samples lie below the two-pass response and in the ND the four-pass response lies below the three-pass response. This result may seem unusual because it is commonly believed that ECAE strengthens most materials with pass number. For instance, Chinh et al. [20] report that the 0.2% compression yield stress (and in tension as well) of pure Al in the ED increases with pass number and saturates after four passes (route Bc). However, in 1050 Al processed using dissimilar channel angular pressing (DCAP) (similar to route A), $\Phi = 120°$, it was found that the hardness decreased after four passes. Generally direct comparisons between our results and yield stresses measured at 0.2% strain in the literature cannot be made because the stresses in Fig. 2 are still rising at 0.2% strain. It is clear, however, that Al does not continue to strengthen after a few passes. Additionally our results demonstrate that changes in material strength with pass number depend on direction of straining.

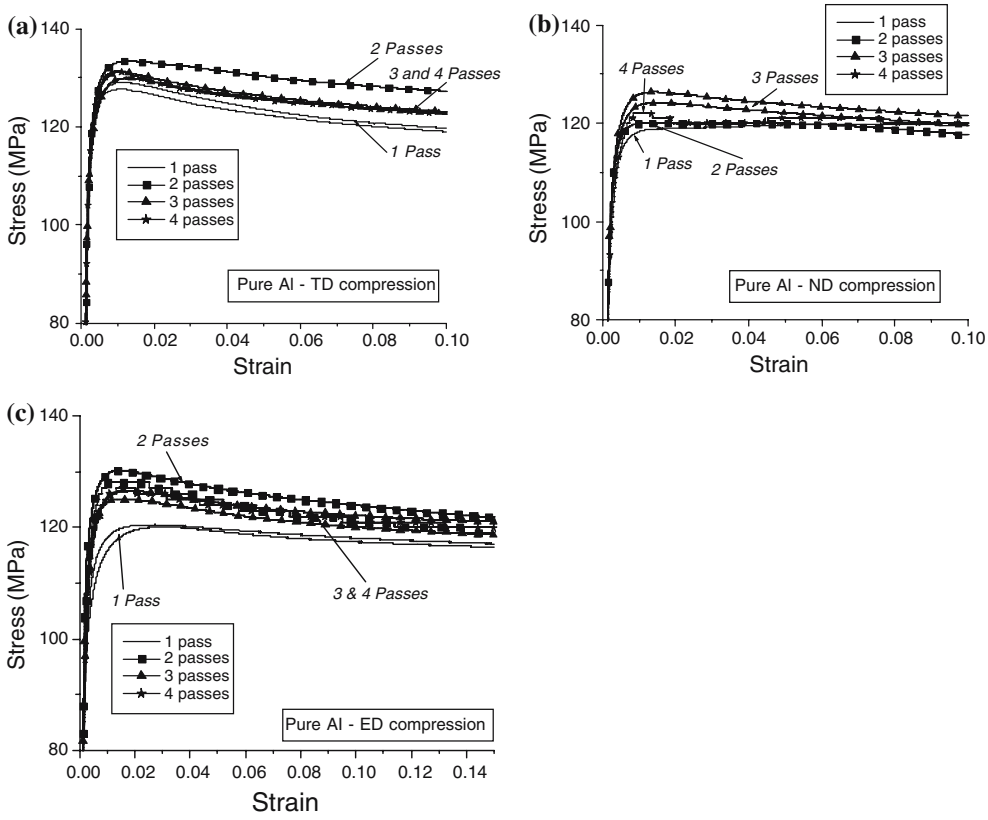

Fig. 2 The flow response of ECAE-processed Al when compressed in the (**a**) TD, (**b**) ND, and (**c**) ED directions after multiple passes of route Bc

In none of these responses do we observe work hardening. Instead the flow stress rises quickly to a maximum value and decreases with further straining. In the TD, this work softening response is observed after all passes. In the ED, work softening is also observed and is more pronounced after multiple passes than the first pass. In the ND, the first- and second-pass samples show some work hardening in the first 5% of straining, but by the third and fourth pass, samples show noticeable work softening. Larger pass numbers in route Bc have been tested by other researchers but usually only in the ED direction. Similar to our observations, eight-pass samples of pure Al, commercial purity Al, and Al alloys alike exhibited a rapid rise in flow stress followed by either no work hardening or work softening [3, 20, 21].

Figure 3 a–c shows, respectively, the compression responses of the Cu samples from 1–16 passes in each of the three directions, TD, ND, and ED. Unlike the Al, strengthening with pass number occurs in each straining direction. The only exception is the 16-pass sample which is slightly weaker than the eight-pass sample in the ED. Dalla Torre et al. [22] also found that their 12-pass and 16-pass pure Cu samples were weaker than their eight-pass sample (also using route Bc and $\Phi = 90°$) when compressed in the ED direction. In tension, Han et al. [23] report that the strength decreased from six to eight passes (route Bc). Considering another route and Φ, route C and $\Phi = 120°$, in Shin et al. [24] the ED-compression strength decreased after four passes.

Multiple inflection points are observed in all the Cu responses indicating transient behavior induced by strain-path changes from multiple shearing (ECAE) to uniaxial compression. Compared to Al, it is easier to identify relationships between the direction of compression, the final strain path, and subsequent hardening characteristics in the Cu. The TD responses consistently and clearly exhibited a work softening response typical of a cross effect: an initial jump in stress followed immediately by a high degree of work softening. In the one- and two-pass samples, the material eventually work hardens after 15–20% of compression straining. However, following more passes, resumption of work hardening is not observed after 25% straining. In the other two directions, this cross effect was not as pronounced. The ND response showed slight work hardening in the first few passes and reducing to nearly zero hardening as the pass number increased. The ED response exhibited a characteristic reversal response [25–28] with an initial concavity followed by an extended transient region of little to no hardening

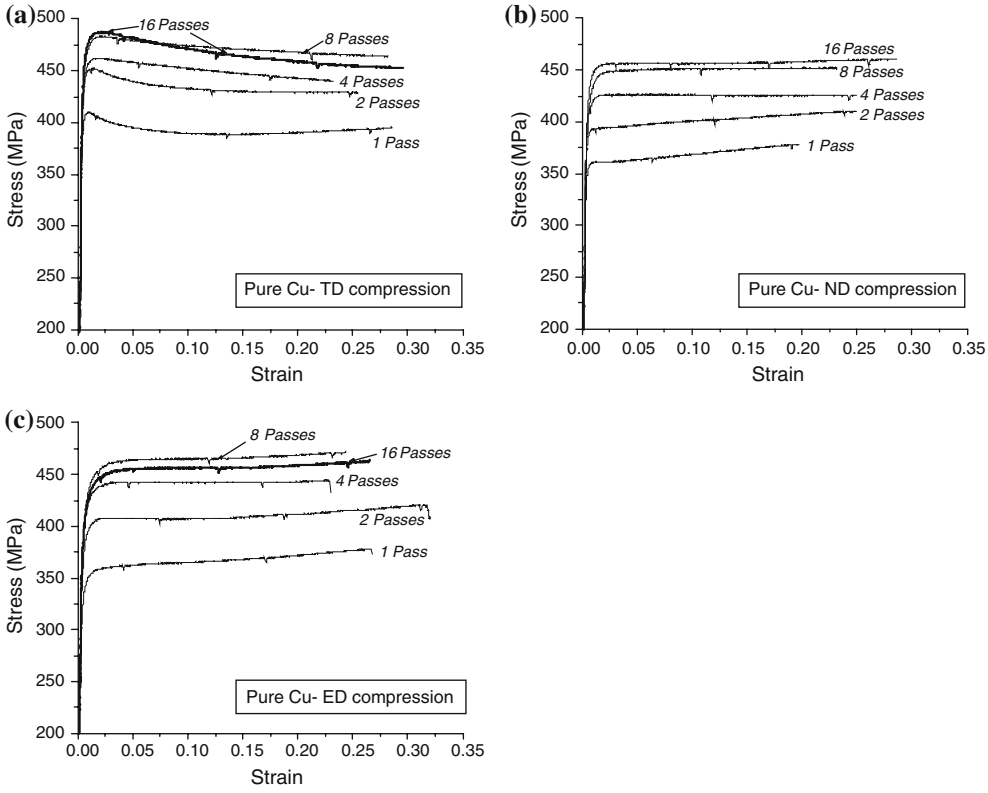

Fig. 3 The flow response of ECAE-processed Cu when compressed in the (**a**) TD, (**b**) ND, and (**c**) ED directions after multiple passes of route Bc

which ends with slight work hardening. Interestingly, these hardening characteristics particular to each direction of straining repeat after each pass, seeming to depend little on pass number.

The order of flow stresses among the three directions evolves similarly with pass number in the two materials, Al and Cu. After the first pass, TD > ND > ED and after subsequent passes, TD > ED ≥ ND. This result is perhaps not surprising considering that these two pure fcc cubic materials share many basic features in their texture and microstructure development, were processed with the same ECAE die (Fig. 1), and both initial textures were weak. Li et al. [29] studied the texture development of these Al and Cu samples up to four passes. The first-pass textures had some differences, but with subsequent passes, the textures became more similar. Komura et al. [30] discussed differences in the microstructural development in pure Al and Cu processed using route Bc and a 90° die. After the first pass, the microstructures both consisted of banded subgrain structures and after multiple passes, they became equi-axed. Evolution to the desired equi-axed substructure of nearly refined grains with high-angle boundaries, however, was much faster in the Al (after four passes) than in the Cu (beyond 10 passes). While the substructure morphology may be similar, the character of subgrain/new grain boundaries and dislocation mobility (e.g., propensity for cross-slip) are different between these two materials. Thus, we can still expect differences in their transient behavior in reloading, such as an initial spike in flow stress, degree of work softening, and extent of transient regions before work hardening resumes.

Particularly in route Bc, the texture and microstructure in these materials change substantially within the first four passes [17, 29–31]. Therefore, the anisotropy and hardening characteristics can also change from pass to pass. Indeed in the Al samples, work softening manifested in nearly all directions and after all passes, with no clear dependence on straining direction. In the Cu, on the other hand, hardening characteristics are particular to the direction of straining but seemingly insensitive to pass number (up to 16). This trend in the Cu signifies that the reload response is largely governed by activation of transient mechanisms defined by the orientation relationship between the reload direction and the deformation of the most recent ECAE pass.

Cross-test effects

When the strain path is changed orthogonal to the pre-strain direction, the reload response of some materials exhibits a ‘cross effect’. A cross-test effect is marked by

an initial spike in flow stress followed by immediate work softening until the flow stress resumes the monotonic response (see Fig. 4). Generally, transient softening in cross-test responses after such large pre-strains is not well understood [32].

Regarding our compression reloads, such cross effects are most obvious in the TD responses, but could also be operative locally in some grains in the other straining directions. One possible explanation is texture (geometric softening). Prior studies on geometric effects in isolation [7] showed some evidence of slight softening in TD after one or multiple passes of ECAE. However, the predicted geometric softening was not nearly as drastic as seen in the data of Figs. 2 and 3. Another reason for work softening could be the formation of localized macroscopic shear bands, an interactive geometric-microstructural component. However, no clear correlation between initial cross effect and shear banding can be made with the available data in the literature. Although the authors in [33] did not observe macroscopic work softening, their optical evaluations revealed shear banding during post-compression of an ECAE Al sample along its axis. In contrast, our Al and Cu samples, which clearly exhibit work softening, had no macroscopic shearing banding. Metallographic analysis of one-pass ECAE and post-compression samples showed no localized deformation at the macroscale. Other explanations include saturation of work hardening or grain boundary sliding. These explanations would explain an ideally rigid plastic response or zero hardening, but not work softening.

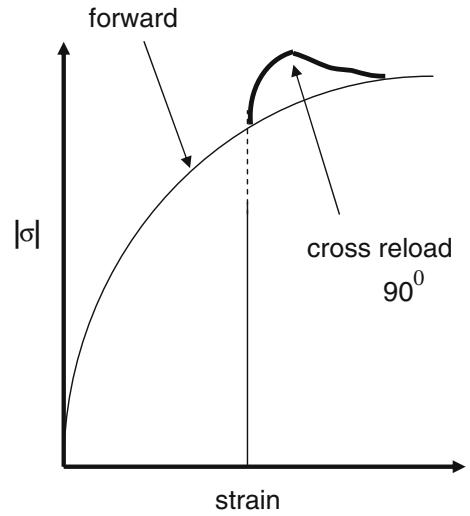

Fig. 4 Schematic of one possible strain-path-change effect on the response of a soft single-phase metal when reloaded 90° to the pre-strain direction. In this illustration, the cross-reload response (solid thick line) has an initial jump in stress followed by work softening to the extrapolated forward response

Also grain boundary sliding is characteristic of fine-grained materials with high-angle boundaries [34]. This requisite microstructure is not yet achieved in the ECAE material after one or a few passes, yet noticeable work softening occurs in these samples.

The final explanation for work softening provided here is the attempt of new slip systems to permeate and annihilate previously developed microstructure [e.g., 25, 35, 36]. Once the structure is dissolved, these 'cutting' dislocations can propagate as usual and work hardening recommences. Dislocation cells, planar dislocation boundaries, and deformation band structures could be dissolved in this process. The directionality of work softening in the Cu up to several passes, would suggest that the primary cause is the formation and dissolution of long planar walls in Cu, structures which fall closely along crystallographic planes. In Al, however, the uniformity in work softening after multiple passes likely coincides with the formation and dissolution of equi-axed structures (cells and/or subgrains) or deformation bands, structures which do not lie along crystallographic planes. Regardless, if there is indeed a dependency on substructure development, then the transient work softening will be negligible unless the primary path generates relatively stable dislocation boundaries, which requires large pre-strains. This trend is supported by observations for example in [35, 37–39]. Generally this mechanism, as well as others considering annihilation of previously stored dislocations, are the most likely explanations for transient work softening (observed after one or two passes).

Although speculated upon quite often, this cut-through and annihilation phenomenon has not been sufficiently modeled in fcc materials in comparison with bcc steels. At the continuum level, formulations for the decay of a macroscopic strength component due to substructure dissolution [25, 37] have been successful at predicting work softening in IF steels in ideal cross-load tests. In a single-crystal hardening model for bcc IF-steel [35], the authors accounted for the trapping of polarized dislocations in dislocation walls. If the deformation was reversed these polar dislocations would become mobile and annihilate the cellular structures. An fcc version of the model [39] accounted for this same reduction, but no work softening was predicted for pre-rolled Cu, reloaded in compression, although it was observed. The Peeters et al. [35] model also included an expression for the decay of pre-existing dislocation boundaries, but because it made flow stress predictions dependent on the simulation time-step, it was not used in the fcc version of the model [39]. Following this work, a cut-through model for fcc metals was developed [40] which assumes that

cut-through was achieved when planar slip prevailed on a slip plane after the strain-path change. This model and its criterion for activating cut-through was later improved [18] and is the one used here.

Reversal test effects

Another strain-path change effect which leads to transients in flow stress and work hardening is the reversal effect. The reversal effect is characterized by a multi-stage flow response as shown in Fig. 5.

Primary stage (A–B) (Bauschinger effect): The reverse flow response begins to show deviations from linearity at point A, and then rapidly rises close to prior stress levels at point B. Definitions of a ''reverse yield stress'' vary widely among studies, but most of them seem to lie within this stage. These include the stress at point A, point B, the Bauschinger strain (the reverse strain to achieve the highest stress in the forward direction), or the stress at 5% reverse strain. Point A consistently falls 10%–20% below the stress achieved at the end of forward straining, irrespective of pre-strain level and material. This is commonly known as the Bauschinger effect. The remaining stages, however, vary with material, pre-strain, and deformation mode.

Secondary stage (B–C): This stage is characterized by work softening from B to C and is not consistently observed. It occurs more often in metals with medium to high stacking-fault energy (SFE), especially after relatively large forward strains. The work softening in reversal is different than that seen in the cross effect.

Tertiary stage (C–D): This stage is characterized by an extended region of zero or little work hardening. As the pre-strain increases, the strain interval of the tertiary stage (C–D) tends to lengthen and its hardening rate to decrease (approaching zero). This long plateau region has been associated with accumulation of polarized dislocations gliding non-coplanar to walls (interstitial-free (IF) steel) [35] or the dissolution of substructure, such as cell walls and extended planar walls (aluminum) [41] or rearrangement of the microstructure [42]. However, the recent work by Vincze et al. [27] in both IF-steel and Al, showed that this stage of the Bauschinger effect can manifest without evidence of cell dissolution or prior wall formation. Microstructural dissolution is, therefore, a likely consequence, but is not the mechanism leading to the long plateau region.

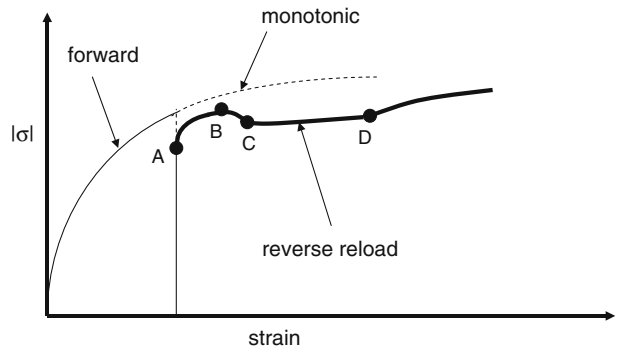

Fig. 5 Multiple stages, A–D, of the flow response after a reversal reload (solid thick line). The forward and reversal responses are plotted as the absolute value of the stress versus total strain

Final stage (D): In this stage, work hardening resumes at D. Observations of reverse responses after D are varied and seem to depend on the test mode (axial versus shear reversal), pre-strain, and material. In some cases, the hardening rate resumes but the flow stresses lie below the extrapolated forward response. The minimum difference has been termed 'permanent softening'. In other cases, the reverse flow response surpasses that in the forward direction, as in the reverse shear response of Cu and Al alloys in Stout and Rollett [26] or the reverse axial responses of some aged Al alloys in [42]. Reversal path changes can therefore have lasting alterations on material response, particularly after large pre-strains. The texture and microstructure formed during preload most likely induce slip activity during a reversal that is very different from what would be the slip activity in the forward load test when continued to the same total strain. As a consequence, grain reorientation and subsequent structure formation would also be different and the monotonic response would not be recovered. Any model wanting to reflect such macroscopic data needs to account for texture, in addition to microstructural changes.

These stages are apparent in the ED-compression responses of a wide variety of ECAE materials reported in the literature [3, 20, 21, 43] and here in Figs. 2c and 3c. Although not a pure reversal, this test direction is closer to a reverse strain-path change with respect to the ECAE sample, compared to compression in other directions.

Mechanisms responsible for a reversal effect are different than those discussed previously for the cross effect. The reversal reload response is governed by the reverse motion of dislocations, some of which are already present in the grain from the previous strain path and available to aid deformation in reverse [27, 41]. These excess dislocations were previously either immobilized by internal stresses or trapped in the substructural network. Any post-ECAE heat-treatment that eliminates these populations of available dislocations would therefore remove any signature of a

reversal effect. Features characteristic of reversal effects observed in the as-processed compression response of an 8-pass route Bc sample of an Al alloy were eliminated after an intermediate anneal [21].

Modeling approach

Modeling anisotropy after large pre-strains, such as ECAE, presents a challenge for it requires describing in a reliable way the concurrent evolution of texture and dislocation structures inside the grains. In previous work [18] we developed a micro-scale constitutive law that relates changes in slip activity, defined by the magnitude and direction of slip on each slip plane, to changes in hardening within each grain in a polycrystal. Accounting for the crystallographic directionality is an important feature of this hardening model, for it allows application to any arbitrary strain-path change. The model treated separately the mechanisms underlying the cross effect and reversal effect. Under arbitrary strain-path changes, such as those in mechanical testing of ECAE pre-strained samples, the polycrystal can have some grains undergoing reversal path changes and others cross-effect changes or both. Only a microscopic model can potentially evaluate the mechanisms responsible for the transient features in the flow response of ECAE materials and what to expect under different ECAE deformations, subsequent test directions and modes. We implement our single crystal constitutive model [18] into a visco-plastic self-consistent (VPSC) polycrystal model [44, 45] and apply the combination to analyze the differences in reload response between the one-pass Al and Cu samples (Figs. 2 and 3). We briefly review the model in this section, mainly to convey the assumptions, physics, and model parameters.

Polycrystal modeling

VPSC is used to relate the plastic response of a polycrystalline material, modeled as a collection of grains each with a distinct crystallographic orientation and volume fraction, to the deformation of the individual grains [44, 45]. It neglects the elastic contribution and in this work, the only deformation mechanism is slip. Calculation of individual grain stresses and strains begins by treating each as an ellipsoid embedded in a homogeneous effective medium with average properties of all the grains. In each increment the visco-plastic compliance of the polycrystal is determined self-consistently. Each grain deforms depending on its interaction with the homogeneous medium, the applied deformation, its shape evolution, and a visco-plastic flow rule, which can account for the directional anisotropy in slip. As a consequence, it is not necessary for each grain to activate at least five slip systems (as in a Taylor model).

In VPSC, the rate-dependent visco-plastic constitutive law or flow rule employed between the grain strain rate $\dot{\gamma}^s$ and grain stress σ [46] is as follows:

$$\dot{\gamma}^s = \dot{\gamma}_0 \left| \frac{m^s : \sigma}{\tau_c^s} \right|^n \mathrm{sign}(m^s : \sigma) \tag{1}$$

where $\dot{\gamma}_0$ is a normalizing strain rate, m^s and τ_c^s are the Schmid tensor and the slip resistance for slip system s, and n is a model parameter[1]. In Eq. (1), $\mathrm{sign}(m^s{:}\sigma) = 1$ if $m^s{:}\sigma$ is positive and –1 if it is negative. Slip will occur in slip system s when the resolved shear stress $m^s{:}\sigma$ approaches the threshold τ_c^s. In this work, the τ_c^s will evolve with straining and changes in strain activity. Polycrystal hardening will thereby have two contributions, one from grain orientations (texture) and the other from the evolution of τ_c^s with strain inside each grain.

Strain measures

A common measure of accumulated shear in a grain is Γ, calculated as the sum of the accumulated shears on all slip systems:

$$\Gamma = \int_0^t \sum_s |\dot{\gamma}^s| \mathrm{d}t \tag{2}$$

Here $\dot{\gamma}^s$ is the shear rate on s calculated using Eq. (1) and is a scalar quantity which can be positive or negative. While Γ is a useful quantity for some hardening laws under monotonic straining, it is not sufficient for modeling hardening transients under strain-path changes. It does not provide a sense of direction or information regarding the distribution of slip activity within a grain. For this reason, we also use directional shear vectors which measure the direction and magnitude of shearing on a slip plane. In doing so, we associate the activity of an individual slip system with its slip plane instead of considering it individually. For fcc Cu and Al, we consider the three slip systems on each of the four {111} planes as a group. The {111} planes will be designated as α, $\beta = 1, 2, 3, 4$.

[1] The exponent n is set equal to 20 and $\dot{\gamma}_0$ is set equal to the macroscopic strain rate. As a consequence strain rate effects induced by n are removed. They can be introduced into the slip resistance, τ_c^s, if desired.

A shear rate vector $\dot{\bar{\nu}}^{\alpha}$ and shear vector $\bar{\nu}^{\alpha}$ can be defined for each slip plane α:

$$\dot{\bar{\nu}}^{\alpha} = \sum_{s\in\alpha} \bar{b}^{s}\dot{\gamma}^{s} \quad \text{and} \quad \bar{\nu}^{\alpha} = \int_{0}^{t} \dot{\bar{\nu}}^{\alpha} \mathrm{d}t \tag{3}$$

where $\bar{b}^{s}$ is the normalized Burgers vector of slip system s expressed in crystal axes, such that the vectors are independent of crystallographic rotations. The bar above the symbol indicates that the quantity is a vector. The magnitudes of the shear rate and shear are defined by the norms of $\dot{\bar{\nu}}^{\alpha}$ and $\bar{\nu}^{\alpha}$:

$$\dot{\nu}^{\alpha} = ||\dot{\bar{\nu}}^{\alpha}|| \quad \text{and} \quad \nu^{\alpha} = ||\bar{\nu}^{\alpha}|| \tag{4}$$

Total scalar shear rates and shear are defined as sums over the plane-specific ones:

$$\dot{\nu} = \sum_{\alpha=1}^{4} \dot{\nu}^{\alpha} \quad \text{and} \quad \nu = \sum_{\alpha=1}^{4} \nu^{\alpha} \tag{5}$$

Anisotropic single-crystal hardening

In the presence of planar dislocation walls the τ_c^s values will vary from slip system to slip system depending on their relative orientation with respect to them. Because dislocation walls are by nature planar, it is reasonable to simplify the model by considering activity in and interactions between slip planes rather than individual slip systems. The three slip systems contained on slip plane α, $s\in\alpha$, will have the same slip resistance, denoted as τ_c^{α}.

$$\tau_c^s = \tau_c^{\alpha}, \qquad s \in \alpha$$

In the remainder of the paper, we will refer only to τ_c^{α}.

In VPSC grain inhomogeneities induced by deformation microstructure are accounted for by the anisotropic evolution of τ_c^s in Eq. (1). τ_c^{α} contains several components:

$$\tau_c^{\alpha} = \tau_h^{\alpha} + \Delta\tau_{\text{cut}}^{\alpha} + \Delta\tau_{\text{rev}}^{\alpha} \tag{6}$$

Each term depends on the local slip activity in the grain, represented by one or a combination of the strain measures in Eqs. (2)–(5). We briefly review their evolution equations and criterion for their operation below.

The first term τ_h^{α} represents the contribution due to dislocation generation, multiplication, and dynamic recovery under multiple slip conditions. It is responsible for the conventional multi-stage work hardening (Stages II–IV) and operates during every deformation path. In single slip, the slip resistance $\tau_{\text{V}}(\Gamma)$ evolves with the accumulated strain in each grain Γ according to the extended Voce law [47]:

$$\tau_{\text{V}}(\Gamma) = \tau_0 + (\tau_1 + \theta_1\Gamma)[1 - \exp(-\theta_0\Gamma/\tau_1)] \tag{7}$$

Note that we implicitly assume that the parameters τ_0, τ_1, θ_0, θ_1 are equal for all slip systems. Being material-dependent, they will be different for Al and Cu (See Table 1). Under multiple slip, the strength of slip system s contained on plane $\alpha(s\in\alpha)$ evolves with the strain rate on its plane and that of the other slip planes β by:

$$\dot{\tau}_h^{\alpha} = \frac{\partial\tau_{\text{V}}}{\partial\Gamma}\hbar^{\alpha\beta}\dot{\nu}^{\beta} \tag{8}$$

Slip interactions which contribute to τ_h^{α} are addressed by a latent hardening model for $\hbar^{\alpha\beta}$. In [18, 48], we propose $\hbar^{\alpha\beta}$ in Eq. (8) to evolve with deformation according to:

$$\hbar^{\alpha\beta} = (1 - h_{\text{sat}})e^{-\delta^{\alpha\beta}} + h_{\text{sat}} \tag{9}$$

where $\delta^{\alpha\beta} = \eta|\nu^{\alpha} - \nu^{\beta}|$ depends on the difference in the accumulated shear on planes α and β (Eq. (4)) and η is the rate at which $\hbar^{\alpha\beta}$ changes from 1.0 (isotropic) to a saturation value h_{sat}.

Deviations of $\hbar^{\alpha\beta}$ from 1.0 provide anisotropic hardening, which in Eq. (9) increases with strain. Considering that latent hardening follows from dislocation interactions, it is reasonable to believe that it will be tied to the formation of the finer scale deformation structures (10^{0}–10^{-3} μm). After small strains, the grain microstructure is relatively weak, consisting mainly of a 3D network of cells formed by statistical trapping and with low misorientations (< 1°). This structure will lead to isotropic hardening as all systems are likely to encounter resistance from them. After large strains, sheet-like dislocation boundaries form more or less aligned to the active slip planes [49] which lead to anisotropic hardening $\hbar^{\alpha\beta} \to h_{\text{sat}}$. When the active systems harden faster than latent ones, characterized by $0 < h_{\text{sat}} < 1$, slip on other planes, such as cross-slip, is promoted. This case of 'slow latent hardening' or when $\hbar^{\alpha\beta} < 1$, has been observed in some single crystal latent hardening experiments of Al and Cu [50–53]. Because cross-slip is more likely in Al than Cu (due to its higher SFE), we set h_{sat} lower in

Table 1 List of model parameters that govern the evolution of the slip resistance τ_h^α related to work hardening

Test	Shear modulus μ [GPa]	Grain size [μm]	τ_0 [MPa]	τ_1 [MPa]	θ_0 [MPa]	θ_1 [MPa]	h_{sat}	η
Al-ECAE reload	26	120	50	11	175	5	0.2	100
Cu-ECAE reload [8]	42	90	20	175	440	26	0.6	100

Al (0.2) than in Cu (0.6). For simplicity, $\eta = 100$ for both. Further discussion on the experimental and theoretical evidence supporting the notion of slow latent hardening and the various scenarios treated by the latent hardening model in Eq. (9) can be found in [18, 41].

The second term $\Delta\tau_{cut}^\alpha$ is the enhancement in slip resistance when newly activated slip activity α must penetrate through dislocation walls, i.e., all planes $\beta \neq \alpha$ (See Fig. 6a). These planar dislocation structures, generated in prior deformation, act as barriers to new slip activity. Consequently new slip activity experiences a rapid but temporary hardening. With continued slip, new dislocations permeate through, leaving less slip resistance for the slipping dislocations behind them. Therefore, the strength enhancement $\Delta\tau_{cut}^\alpha$ decays if the new slip activity persists.

This cut-through mechanism, unlike latent hardening, becomes apparent when there is a significant change in slip activity within the grain. Activation of this cut-through mechanism depends on both prior deformation on the previously active slip plane β and new slip activity on α, non-coplanar to $\beta(\beta \neq \alpha)$. As explained in [18] and illustrated in Fig. 6a, this mechanism is activated within the model for new slip activity α, if the following criterion is satisfied:

$$X^{\alpha\beta} = \left|\left|\frac{\dot{\bar{\nu}}^{\alpha,n+1}}{\dot{\nu}} \times \frac{\bar{\nu}^\beta}{\nu}\right|\right| - \left|\left|\frac{\dot{\bar{\nu}}^{\alpha,n}}{\dot{\nu}} \times \frac{\bar{\nu}^\beta}{\nu}\right|\right| > X_c = 0.15 \qquad (10)$$

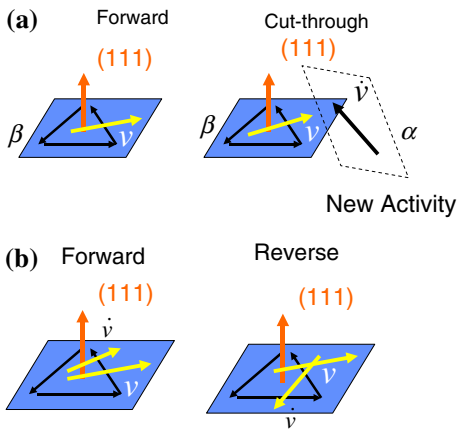

Fig. 6 Examples of changes in slip plane activity ($\dot{\bar{\nu}}^\alpha$) which activate (**a**) cut-through mechanisms or (**b**) reversal mechanisms

The initial extra stress $\tau_{cut,0}^\alpha$ required for dislocations associated with newly activated slip systems on α to overcome all possible dislocation boundaries β, non-coplanar to it ($\beta \neq \alpha$), is:

$$\tau_{cut,0}^\alpha = \sum_{\beta \neq \alpha} X^{\alpha\beta} \tau_d^\beta \qquad (11)$$

where in Eq. (11), $X^{\alpha\beta} = 0$ if $X^{\alpha\beta} < X_c$. τ_d^β is associated with the strength of the boundary β, being penetrated. We begin with a general form derived from dislocation dynamics [54] and modified in [18], as follows:

$$\tau_d = 0.086 \mu k_c v_{cut}^\beta \ln\left(\frac{1}{k_c v_{cut}^\beta}\right) \qquad (12)$$

where μ is the shear modulus, and the material constant k_c is on the order of 10^{-2}. In [18], we introduced a shear measure v_{cut}^β which is inversely related to the dislocation spacing d in the boundary. Let v^β be the shear accumulated on plane β up to the point that $X^{\alpha\beta} > X_c$ is satisfied. We envision that b/d increases with v^β, according to the non-linear relationship in Fig. 7, where the parameter v_1 represents the strain at which dislocation walls begin to form and v_2 the strain at which they have become stabilized. The empirical relationship in Fig. 7 can be expressed as:

$$v_{cut}^\beta = \frac{1}{1 + \exp(-2v^{\beta*})} \quad \text{where}$$
$$v^{\beta*} = (2v^\beta - v_2 - v_1)/(v_2 - v_1), v_2 > v_1 \qquad (13)$$

In this model, the reduction of $\Delta\tau_{cut}^\alpha$ represents the process of localized removal of subgrain boundaries that developed during pre-deformation:

$$\Delta\dot{\tau}_{cut}^\alpha = -\omega \Delta\tau_{cut}^\alpha \dot{\nu}^\alpha, \qquad (14)$$

where ω is a material parameter related to the ability of dislocations to punch through or overcome the boundaries. In the above, the rate of removal is proportional to the remaining strength $\Delta\tau_{cut}^\alpha$ and to $\dot{\bar{\nu}}^\alpha$ the active shear rate on α. A higher $\dot{\bar{\nu}}^\alpha$ indicates a higher flux of dislocations available for dissolving the

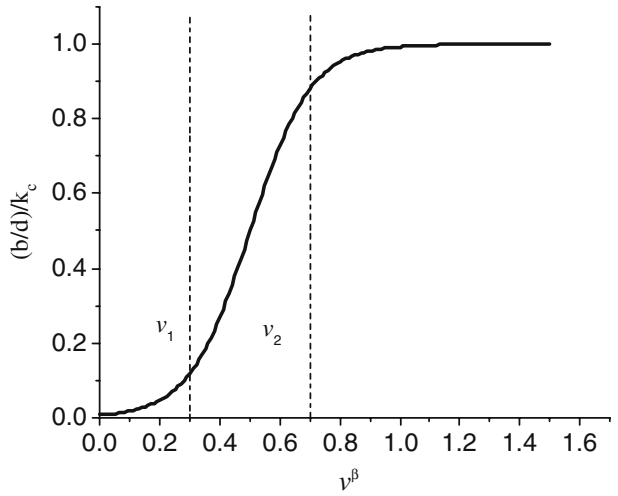

Fig. 7 Relationship between the boundary quantity $(b/d)/k_c = v^{\beta}_{\text{cut}}$ along plane β and the accumulated shear on plane β, v^{β}. The meaning of v_1 and v_2 are also shown. See Eq. (13)

boundary. Solving Eq. (14) assuming $\Delta\tau^{\alpha}_{\text{cut}}(0) = \tau^{\alpha}_{\text{cut},0}$ yields an exponential decay.

Once the initial enhancement ${\tau_{\text{cut},0}}^{\alpha}$ is removed, the work softening effect will cease and work hardening will dominate the grain response. However, new slip activity can also dissolve other weaker portions of the microstructure, like dislocation cells. While these features may not contribute to the initial spike at the instant of an activity change, their dissolution may lengthen the work softening effect to strains beyond those required to only remove $\tau^{\alpha}_{\text{cut},0}$ in Eq. (11) associated only with planar boundaries. This additional dissolution process can be represented in Eq. (14) as additional slip barriers $\Delta\tau_{\text{other}}$ that are dissolved:

$$\Delta\dot{\tau}^{\alpha}_{\text{cut}} = -\omega\left(\Delta\tau^{\alpha}_{\text{cut}} + \Delta\tau_{\text{other}}\right)\dot{v}^{\alpha} \tag{15}$$

Note that in the cut-through model Eqs. (10–15), barrier walls are treated as permeable. Therefore hardening after a strain-path change will be more sensitive to the strength of the barriers created in pre-loading than to the exact orientation of the barriers with respect to the direction of new slip (e.g., mean free path). Also, slip interactions are simplified to coplanar versus non-coplanar relationships. Calculating more precise crystallographic relationships between slip systems and substructure requires knowledge of the orientation of the boundaries, which can vary greatly from grain to grain in Al and Cu [15, 16, 39, 49]. Results from Al and Cu single-crystal latent hardening experiments suggest that hardening was not very sensitive to the orientation change associated with the strain-path change [51, 52].

The last term $\Delta\tau^{\alpha}_{\text{rev}}$ is the strength reduction due to the reverse glide of a fraction of the dislocations generated during forward motion. Slip activity on plane α reverses its sense when the following criterion is satisfied [40]:

$$P^{\alpha\alpha} = \frac{\bar{v}^{\alpha}}{v}\cdot\frac{\dot{\bar{v}}^{\alpha}}{\dot{v}} < 0 \quad -1 \le P^{\alpha\alpha} \le 1 \tag{16}$$

An illustration of a slip plane reversal which satisfies Eq. (16) is found in Fig. 6b. $\Delta\tau^{\alpha}_{\text{rev}}$ becomes non-zero when Eq. (16) is first satisfied.

As demonstrated in [18], the reversal response of Cu is complex and cannot be explained by one mechanism alone. Accordingly $\Delta\tau^{\alpha}_{\text{rev}}$ will have two separate parts; $\Delta\tau^{\alpha}_{\text{rev}} = \Delta\tau^{\alpha}_{B} + \Delta\tau^{\alpha}_{R}$, each representing a different reversal mechanism. The first leads to transient changes in the initial stage of reverse straining (Stage A–B in Fig. 5) and is due to internal stresses. The second leads to reductions in hardening rate due to dislocation rearrangement and dissolution. This distinction follows conclusions made from detailed experiments [42, 55]. Several reversal studies on pure metals and alloys show that the evolution of each part depends on material, microstructure, and strain history, e.g., [25–28]. For simple cubics like Al and Cu, $\Delta\tau^{\alpha}_{B}$ is prevalent only in the first few percent of reverse straining, while $\Delta\tau^{\alpha}_{R}$ is dominant in the later stages of reverse straining.

Some of the dislocations gliding in reverse were immobilized in forward straining by internal stresses ('backstresses'). Their reactivation in reverse slip is made possible by the change in sign of the applied stress state that becomes more aligned with this internal stress. Their contribution to slip is viewed as a surplus and therefore produces a reduction in the strength by $\Delta\tau^{\alpha}_{B}$. This drop is commonly associated with the Bauschinger effect (stage A–B in Fig. 5). According to evidence provided by X-ray measurements in Wilson and Bate [55], the internal stress state which aids their reverse gliding decays exponentially with reverse straining. Therefore in the model [18], $\Delta\tau^{\alpha}_{B}$ is made to decay according to:

$$\Delta\tau^{\alpha}_{B} = \mu P^{\alpha\alpha}_{0} v^{\alpha}_{\text{rev}} \exp\left(-\frac{v^{\alpha}_{\text{new}}}{v_B}\right) \tag{17}$$

where $P^{\alpha\alpha}_{0}$ denotes the value of $P^{\alpha\alpha}$ at the instant of reversal, v^{α}_{new} is the amount of strain accumulated since the reversal event, v_B is the reverse strain required to nullify the internal stress (usually 0.5% to 3%), and v^{α}_{rev} is a strain measure, related to the amount of dislocations frozen in place by internal stresses generated under the pre-strain v^{α}. The factor

$P_0^{\alpha\alpha}$ is included in the expression for $\Delta\tau_B^\alpha$ to provide orientation dependence. In [55] v_{rev}^α and v_B were found to depend on material, but only the former depended on pre-strain, albeit slightly. To reflect this mild dependence, we set:

$$v_{\text{rev}}^\alpha = v_{B,\text{sat}}(1 - \exp(-_B v^\alpha)). \tag{18}$$

With θ_B on the order of 10, v_{rev}^α quickly saturates to $v_{B,\text{sat}}$ within a few percent of pre-straining v^α. Not surprisingly, $v_{B,\text{sat}}$ is found to be lower for Al than Cu (See Table 3), as ECAE microstructures in Al contain less dislocations in the interior regions between subboundaries than those in Cu.

In single-phase pure metals, such as Al and Cu, or lightly alloyed metals, a large fraction of potentially reversible dislocations are immobilized in forward straining because they are tangled in deformation-induced dislocation structures [28, 41]. When the local strain direction is reversed, they find it easier to glide in reverse and, as reverse straining proceeds, they are slowly released from entanglement. Their reverse motion is also viewed as a surplus and leads to a reduction in strength $\Delta\tau_R^\alpha$. The magnitude and extent of strain over which $\Delta\tau_R^\alpha$ operates depends on dislocation mobility and on how much of these dislocations were originally locked up. Regarding the latter, more reversible dislocations tend to be available with larger pre-strains and/or finer substructural features.

An expression for $\Delta\tau_R^\alpha$ is more complex than $\Delta\tau_B^\alpha$ and is assumed to be proportional to f' the fraction of these dislocations released from entanglement within a substructural network:

$$\Delta\tau_R^\alpha = \mu P_0^{\alpha\alpha} f'\left(v_{\text{new}}^\alpha\right) \tag{19}$$

In previous work [18], we surmised a general form of f' as a function of v_{new}^α:

$$f' = \frac{f'_{\text{peak}}}{g_{\text{peak}}}\left[\exp\left(-\frac{v_{\text{new}}^\alpha}{v_R}\right)\text{Lognormal}(v_{\text{new}}^\alpha|\mu_R,\sigma_R)\right] \tag{20}$$

where g_{peak} is the maximum of the function in brackets. A two-parameter lognormal function is used merely to give f' the appropriate shape. The form of f' estimated for the Al and Cu are compared in Fig. 8. In both, the amount of dislocations initially released increases with reverse straining v_{new}^α but, as only so much is available, f' must eventually decrease. The key features of f' are the material-dependent peak value f'_{peak} (higher for Al than Cu) and pre-strain-dependent tail, which is controlled by the exponential term, $\exp(-v_{\text{new}}^\alpha/v_R)$ in f'. Since the pre-strains for one-pass Al and Cu are the same, the governing decay parameter v_R in this term is the same.

Note that because both $\Delta\tau_R^\alpha$ and $\Delta\tau_B^\alpha$ include $P_0^{\alpha\alpha}$, $\Delta\tau_{\text{rev}}^\alpha$ carries information regarding the degree of reversal experienced by the grain. The closer the activity change is to a pure reversal, the more dislocations are released.

Comparison with experiment

Simulating the ECAE

We apply the modeling approach described above to predict the anisotropic plastic response of Al and Cu after a single pass of ECAE. The prediction accounts for texture evolution, grain shape evolution, interaction of each grain with the surrounding polycrystal (i.e., the anisotropic homogeneous effective medium), anisotropic hardening along active slip planes, reversal effects (such as the Bauschinger effect) and interactions between pre-existing and newly developing substructure. A co-rotation scheme [56] was implemented to calculate crystallographic reorientation. This scheme slows down and disperses texture evolution and provides better agreement with ECAE textures up to 16 passes [57, 58].

Because of the rounded corner of our die (Fig. 1), ECAE deformation is not adequately modeled by simple shear localized at the intersection plane of the two channels. 2-D and 3-D finite element models [59, 60] show that for rounded-corner dies, plastic deformation is spread over a broad zone, called a plastic deformation zone (PDZ). In [61] we divided the PDZ into the two domains shown in Fig. 9 and derived the analytic form of the deformation and velocity gradients in each domain. The upper part, the central fan with internal angle β, is where most of the intense severe plastic deformation occurs by successive shearing on planes that rotate counterclockwise (CCW) in the 1–2 plane of the die[2]. Deformation by the central fan was shown to be homogeneous and dependent only on β, its internal angle [61]. Because we intend to compare our predictions with mechanical tests performed on compression samples cut from the center of the billet, only the velocity gradient associated with the upper fan

[2] The lower part in Fig. 9 consists of localized plastic deformation bounding a region of rigidly rotating material.

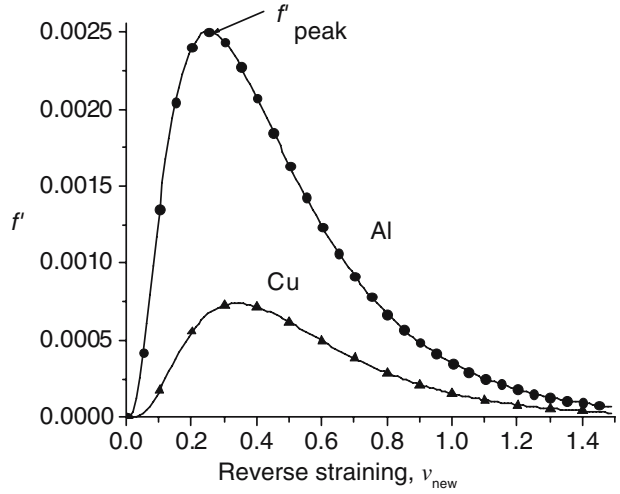

Fig. 8 Comparison of the release functions for reversible dislocations used in the model for Al and Cu

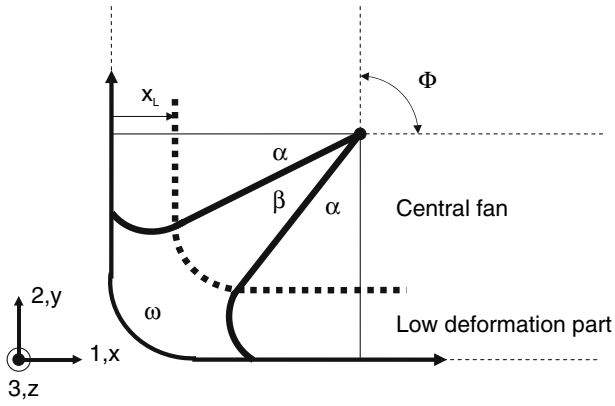

Fig. 9 Schematic of the fan model of Beyerlein and Tomé [61] used to simulate the deformation applied by the ECAE process. This figure is taken from [12]

domain in Fig. 9 is imported into VPSC to describe strain evolution[3].

The texture after single [2, 61] and multiple passes of ECAE [29] develops differently depending on the fan angle β. The CCW rotation in shearing associated with the broad fan deformation ($\beta > 0$) leads to a shift in some of the texture components [61] from their positions established during simple shearing ($\beta = 0$). This signature shift enables characterization of β through comparisons with texture measurement. For the Al and Cu materials processed using the die in Fig. 1, neutron diffraction and FEM-based predictions [12, 29] suggest that $\beta = \pi/10$.

Both the Al and Cu polycrystals are assumed to initially have spherical grains. The Al polycrystal is represented by 1500 randomly distributed orientations. The Cu polycrystal is represented by 1500 distinct orientations distributed according to an OIM measurement of the initial texture [11]. The initial Cu texture is a weak fiber texture, axi-symmetric about the billet long axis.

Model predictions for anisotropy in compression

Figures 10 and 11 compare the model predictions with the compression-reload experiments on the one-pass ECAE Al and Cu, respectively. As in the experiment, a complete simulation involves a single pass of ECAE (assuming $\beta = \pi/10$ in Fig. 9) immediately followed by compression testing in one of the three orthogonal directions. For subsequent compression testing we assume traction-free surfaces perpendicular to the direction of axial compression. The same set of parameters is used when simulating ECAE pre-straining and compression reloading in all three directions. The parameters used for Al and Cu are listed in Tables 1–3. Figures 10 and 11 show that the model effectively predicts the order of flow stresses, degree of anisotropy, and transient behavior in the measurement for both Al and Cu.

After the significant work softening transient in the TD compression response, work hardening is observed to resume in the Cu, but not in the Al. The model predicts resumption of work hardening in both materials, which corresponds to a completion of the process of cutting through planar subgrain boundaries,

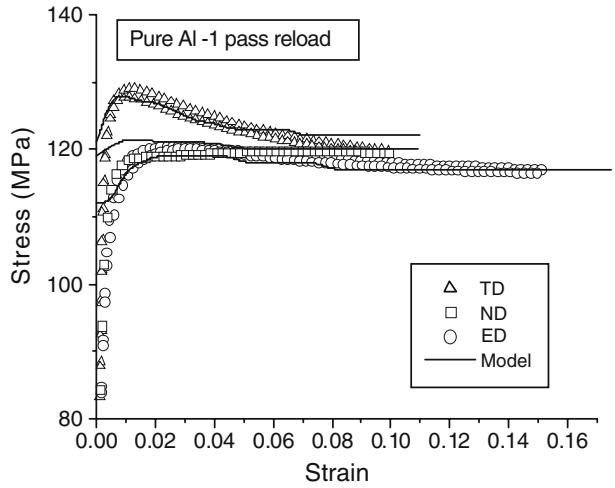

Fig. 10 Comparison between the measured compression reload responses after one ECAE pass and model predictions (solid lines) for pure Al. The model predicts flow stresses in the following order: TD > ND > ED

[3] For the die geometry (Fig. 1), processing conditions, and copper used in [8], the lower part applies to the bottom 10%–20% of the billet.

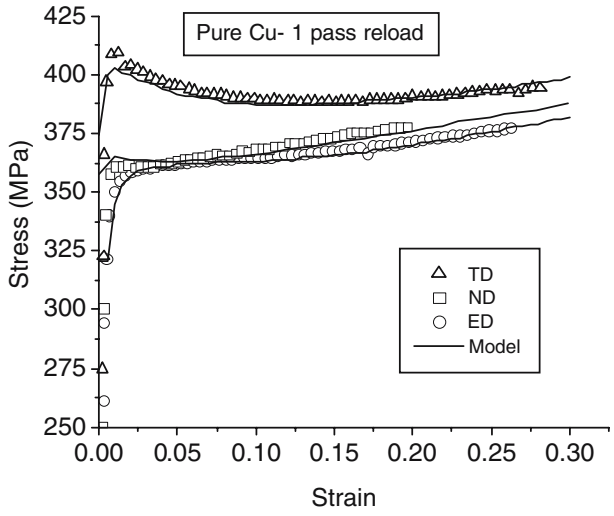

Fig. 11 Comparison between the measured compression reload responses after one ECAE pass [7, 8] and model predictions (solid lines) for pure Cu. The model predicts flow stresses in the following order: TD > ND > ED

Eq. (14). To elaborate on an idea mentioned earlier, other microstructural features can be dissolved in the process. We suspect that this may be happening in the Al leading to an extended work softening regime. After one pass, Al, with a higher SFE, is more likely than Cu to develop an equi-axed substructure, consisting of a mix of cells and subgrains, which has less directional properties. If we use instead Eq. (15), set $\Delta\tau_{\text{other}} = 0.25\Delta\tau^{\alpha}_{\text{cut}}$ and $\omega = 30$ as in the Cu, and repeat the simulation of ECAE plus three compression reloads, we obtain the results in Fig. 12. The work softening effect in the TD response has been extended and the impact on the response in the other two directions is minimal.

Table 4 lists the percentage of grains operating cut-through, or reversal mechanisms, or both for each material and each test. None of the strain-path-change sequences associated with reloading ECAE material in compression represents a pure strain reversal. Each test direction induces in the polycrystal a different combination of cross (cut-through) and reversal mechanisms. As shown, both materials operated similar mechanisms for the same test. A larger number of grains in ED than in ND and TD undergo reversal. Because of this, all stages of the reversal effect are apparent in the ED response. All directions activate cut-through mechanisms with the largest percentage in the TD, followed by ND and ED. Because compression along the TD includes more cross mechanisms, the work softening shortly after reloading in TD is more pronounced than in the other directions. A small fraction of grains in the ED and TD had both mechanisms operative, which means that at least one of their slip planes satisfied $1/3 < \tau^{\alpha}_{\text{cut}}/(\tau^{\alpha}_{\text{rev}} + \tau^{\alpha}_{\text{cut}}) < 2/3$. Clearly when modeling reload responses of ECAE samples, it is important to allow for different mechanisms to operate within each grain.

Reversal effects are an important mechanism in two straining directions, TD and ED. In the model, the $\partial\Delta\dot{\tau}^{\alpha}_{R}$ associated with f' and the hardening rate associated with dislocation accumulation $\partial\dot{\tau}^{\alpha}_{h}$ together govern the reverse flow response. In particular, work softening manifests when the reduction of $\Delta\tau^{\alpha}_{R}$ (after f'_{peak} is reached) exceeds the work hardening by τ^{α}_{h} (Eqs. 7–9). In both Al and Cu we observe this stage. Although not tested here, the reversal model captures the influence of

Table 2 List of model parameters that govern the evolution of the cut-through strength, $\Delta\tau^{\alpha}_{\text{cut}}$, which enhances the slip resistance

Symbol	Cu	Al	Description
k_{c}	2.3×10^{-2}	0.7×10^{-2}	Dislocation density coefficient
ω	30	40	Rate of cut-through
v_1	0.3	0.1	Strain at which wall formation begins
v_2	0.7	0.5	Strain at which wall formation is completed

Table 3 List of model parameters that govern the evolution of the reversal strength, $\Delta\tau^{\alpha}_{\text{rev}}$, which reduces the slip resistance

Symbol	Cu	Al	Description
μ_{R}	0.25	0.25	Lognormal scale parameter
σ_{R}	0.85	1.00	Lognormal shape parameter
B	15	15	Rate of saturation for reverse shear
$v_{B,\text{sat}}$	2.8×10^{-3}	1.0×10^{-3}	Maximum shear available for Bauschinger effect
f'_{peak}	0.74×10^{-3}	2.5×10^{-3}	Peak value in release rate function
v_B	0.01	0.01	Strain for decay of internal stress
v_{R}	0.4	0.4	Measure of pre-strain in release rate function

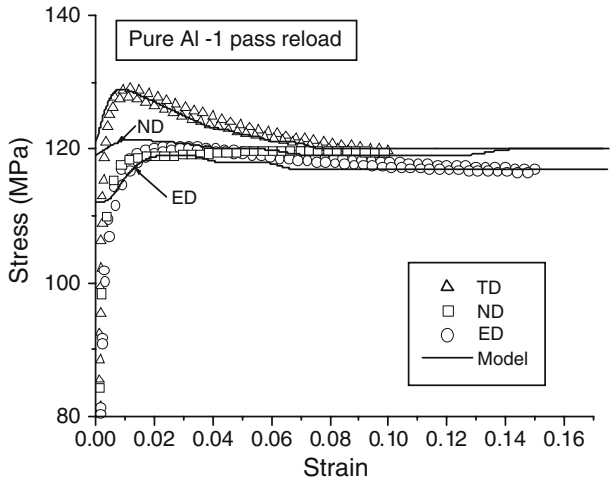

Fig. 12 Comparison between the measured compression reload responses after one ECAE pass and model predictions (solid lines) for pure Al using Eq. (15) instead of Eq. (14) for an extended work softening effect

pre-strain [18] as well. Small pre-strains mean higher $\partial\dot{\tau}_h^{\alpha}$ and faster decay $\partial\Delta\dot{\tau}_R^{\alpha}$, leading to a shorter transient reverse response. Larger pre-strains mean lower $\partial\dot{\tau}_h^{\alpha}$ and slower decay $\partial\Delta\dot{\tau}_R^{\alpha}$, manifesting into noticeable softening (from B–C in Fig. 5) and an extended plateau region (tertiary stage C–D).

Tension–compression asymmetry

The tensile anisotropy results for one-pass Al are presented in Fig. 13 (where the symbols are the measurement). Generally the anisotropy was similar to that in compression, with the TD response being higher than the ED and ND responses. The largest tension–compression asymmetry is found in the ED response, being much higher in tension than compression. The same, but much weaker tension–compression asymmetry is found for one ND sample and no asymmetry for the other. In the other ND sample, there was very little difference between the tension and compression responses. In the TD sample, there is virtually no tension–compression asymmetry.

Using the same parameters as those used in Fig. 12, the simulation was repeated for subsequent tensile tests. The model predictions are shown in Fig. 13. In the TD, little to no tension–compression asymmetry is predicted. In the ND, tension is lower than compression. In the ED, tension is higher than compression. The tension–compression asymmetries in the ED and ND are, however, small. The predicted tension–compression asymmetry in each direction is reasonably consistent with the measurement.

The small asymmetry occurs in spite of the model prediction that the strain-path-change mechanisms were different between the tension and compression tests for a given direction. Compared to the compression responses (Table 4), TD-tension had more reversal grains (17%), ND-tension had significantly more reversal grains (66%), and ED-tension had no reversal grains. The number of grains activating cut-through mechanisms was nearly the same in tension and compression. Activation of the reversal mechanisms in a substantially larger number of grains in ND-tension and ED-compression explains why these responses are lower than those corresponding to the opposite sense of loading.

Discussion

Under compression, our ECAE-processed Al and Cu samples exhibited plastic anisotropy and noticeable changes in hardening characteristics, including no hardening or negative hardening (work softening). These changes in plastic response are the result of strain-path-change effects. As is true with any strain-path change, the severity of these effects depends on the direction of reloading and the texture and dislocation microstructures generated during pre-loading, which is significant when the pre-loading is one or more passes of ECAE. Therefore, transient behaviors in the compression flow response of most as-processed ECAE materials, not just the route Bc samples studied here, can be expected. Any post-heat-treatment to

Table 4 Percentage of grains in the polycrystal which undergo either cut-through or reversal mechanisms during each direction of compression reloading

	Al-ED	Al-ND	Al-TD	Cu-ED	Cu-ND	Cu-TD
Reversal	76.5%	0.0%	10.7%	76.1%	0.0%	12.0%
Cut-through	31.1%	38.2%	74.9%	31.4%	39.4%	79.2%
Mixed	3.4%	0.0%	5.9%	2.9%	0.0%	7.3%

Some grains, denoted as 'mixed' grains, have both mechanisms operative. The criterion for 'mixed' grains is found in the text and is more strict than the formula, % mixed = 100% –(% reversal + % cut-through)

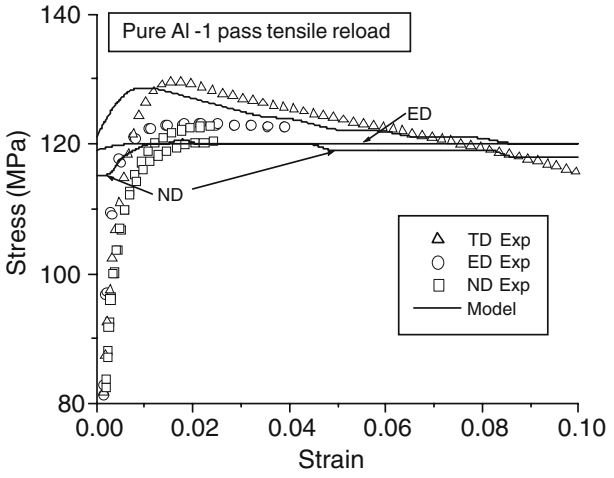

Fig. 13 Comparison between the measured tensile reload responses after one ECAE pass and model predictions (solid lines) for pure Al using Eq. (15) instead of Eq. (14) for an extended work softening effect. The predicted order of flow stresses at 1% is TD > ED > ND

remove the stored dislocations, substructure, or texture generated during ECAE will, however, soften or remove these effects and the usual work hardening will resume, as seen in [21].

While the number of modeling efforts in ECAE is large, very few have addressed anisotropy of ECAE materials [18, 41]. For the ECAE application considered here, we find that there is still insufficient understanding of the anisotropy in the mechanical performance of fcc materials processed to large strains. Most models that predict stress–strain responses after strain-path changes have been applied to experiments involving either smaller pre-strains or simpler loading paths than a single pass of ECAE. Part of the challenge lies in the fact that for ECAE-processed materials, the texture and microstructure, the two main factors determining anisotropy, are significantly different than those of the starting material and can vary widely with processing conditions and material [31]. Another part is that the strain-path changes involved in mechanical testing of ECAE materials are mixed, not pure reversal- or cross-loadings. For simple fcc materials, like Al and Cu, texture evolution in ECAE can be reasonably predicted [31]. Also there have been a few notable attempts to model microstructural evolution during ECAE [62–64]. For plastic anisotropy calculations, additional theoretical elements are required, such as the relationship between local changes in slip activity and anisotropic single-crystal hardening. This relationship is governed by the deformation microstructures generated in pre-straining as well as the dislocation mechanics particular to material and deformation conditions (temperature and strain rate). Undeniably, modeling plastic anisotropy of ECAE materials requires us to introduce microstructural models at the grain- and subgrain-level. To this end, a crystallographically based single-crystal hardening law for strain-path changes that was developed in [18] is applied to mechanical tests performed on single-pass ECAE Al and Cu samples. It provides a relationship between the local slip activity and anisotropic hardening.

Within this model, subgrain deformation microstructures play many roles in determining the directional anisotropy in single crystal hardening. Regardless of which path in the straining sequence is being imposed, dislocations will tend to organize into substructures, which serve to increase the flow stress. The influence of their development with straining during any stage in the deformation is captured by the extended Voce model for single slip and the latent hardening model for coupling in multiple slip (Eqs. (7)–(9)). In contrast, the influence of slip activity reversing its sense of direction or of new slip activity attempting to permeate and locally dissolve pre-existing structure is captured by the reversal and cut-through mechanisms, respectively. These mechanisms consider deformation microstructures to have a transient effect on the flow stress. Changes in hardening characteristics depend on the amount and orientation of old slip activity and new slip activity. When incorporated into our polycrystal model, VPSC, this single-crystal constitutive law is effective in predicting the plastic compression anisotropy of one-pass ECAE material. As demonstrated in this work, in subsequent testing, a polycrystal can have some grains undergo cross-effects, while others experience reversal effects. Particularly under arbitrary strain-path changes, such as axial testing after drawing [38] or rolling [39], it is important to allow for these two mechanisms to operate simultaneously in each crystal of the aggregate.

For each material, Al and Cu, a different set of parameters was used. Some of them were the same for the two materials, particularly those related to preloading, such as v_R, used to determine f' in Fig. 8. Differences between the material parameters are consistent with what is known about their dislocation mechanics. The parameters that govern the evolution for τ_h^α for Al and Cu are listed in Table 1. As explained earlier, the latent hardening parameter h_{sat} related to cross-slip is set lower for Al than Cu, due to the higher SFE in Al. The Voce parameters, associated with the law in Eq. (7), are material parameters that govern the Stages II–IV flow stress and hardening characteristics measured in these materials in their initial state. They are expected to be different for Al and Cu. The

parameters used for $\Delta\tau^{\alpha}_{cut}$ for Al and Cu are listed in Table 2. Al tends to form stable, well-defined sub-boundaries more quickly with straining and pass number than Cu [30]. In accordance, we lower v_1 and v_2 and using the model, estimate that the dislocation density coefficient for walls, k_c, is lower for Al compared to Cu. The breakdown parameter ω is higher for Al than Cu due its greater ease for cross-slip. Last, we summarize the $\Delta\tau^{\alpha}_{rev}$ parameters for Al and Cu in Table 3. Figure 8 compares the estimated release rate function f' for Al and Cu, which contains some of the material-dependent parameters for $\Delta\tau^{\alpha}_{rev}$. Under the same pre-straining conditions (one pass of ECAE), Al has more dislocations available in reversal (area under f' curve) than the Cu. This implies either that it is easier for dislocations in Al to release from sub-boundaries or simply that there are more dislocations available for reverse motion in Al than Cu. It may be expected that the Al with a finer substructure has a higher f'_{peak} than the Cu with a coarser substructure [30]. The difference could also be due to the much higher SFE of Al than Cu [26]. Accordingly, the Al dislocations are more able to rearrange and recover via cross-slip than the Cu dislocations. This suggests that for even lower SFE metals, such as brass, or heavily alloyed metals, it would be more difficult for dislocations to untangle from the substructure, rearrange, or annihilate, in which case, the amount of release would be smaller. Therefore for the same pre-strain, reversal responses of such materials are less likely to have an extended softening regime (B–D in Fig. 5).

Conclusions

In this work, we study the transients in flow response of Al and Cu after one to several passes of route Bc. In most cases, either a reduction of work hardening or work softening is observed. Compression in the TD consistently exhibits an enhanced flow stress followed by immediate work softening, typical of a cross-strain-path change. Compression in the ED likely invokes reversal mechanisms which result in lower flow stresses (i.e., Bauschinger effect) and extended strain periods of little to no hardening. Generally, over all passes, the changes in work hardening in Cu are better defined than in Al.

Tests were repeated in tension for one-pass Al. We find that tension in the TD also leads to work softening and has little difference compared to the compression response. In contrast, tension in the ED has a higher flow stress than in compression in the ED. The opposite occurs in ND, in which the tension response has a lower flow stress.

In this work, we effectively predict the plastic anisotropy of single-pass ECAE Al and Cu samples by applying a crystallographically based single-crystal hardening model [18]. This model relates the changes in hardening to local changes in slip activity for each slip plane in each grain and includes reversal and annihilation of pre-generated substructures. This grain-level constitutive law is imported into a rate-dependent VPSC polycrystal model, that concurrently accounts for texture and grain-shape evolution. Notably, for each material Al and Cu, the simulation employs the same set of material parameters throughout the entire deformation sequence, ECAE followed by axial compression, and in all directions. The set of parameters that are related to dislocation mobility are different for the two materials. These parameters are consistent with the notion that compared to Cu, dislocations in Al more easily cross slip, develop substructures under monotonic loading, destroy them in cross-loadings, and are re-mobilized in reversal. While we apply this model to an ECAE material loaded in compression or tension, we foresee that it can be extended for other subsequent mechanical test modes (e.g., torsion, shear [38, 65]), other ECAE processing schedules, and bulk forming processes in general (e.g., rolling [39, 66]).

Acknowledgements Support by a Los Alamos Laboratory-Directed Research and Development project (No. 20030216) and Office of Basic Energy Sciences Project FWP 06SCPE401 are gratefully acknowledged.

References

1. Segal VM (1995) Mater Sci Eng A197:157
2. Valiev RZ, Islamgaliev RK, Alexandrov IV (2000) Progr Mater Sci 45:103
3. Chinh NQ, Voros G, Szommer P, Horita Z, Langdon TG (2006) Mater Sci Forum 503–504:1001
4. Stolyarov VV, Zhu YT, Alexandrov IV, Lowe TC, Valiev RZ (2001) Mater Sci Engng A 299:59
5. Bengus VZ, Tabachnikova ED, Natsik VD, Mishkuf I, Chakh K, Stolyarov VV, Valiev RZ (2002) Low Temp Phys 28:864
6. Horita Z, Fujinami T, Langdon TG (2001) Mater Sci Engng A 318:34–41
7. Alexander DJ, Beyerlein IJ (2004) In: Zhu YT et al (eds) Ultrafine grained materials III. TMS, Warrendale, PA, pp 517–522
8. Alexander DJ, Beyerlein IJ (2005) I J Mater Sci Engng A 410–411:480–484
9. Haouaoui M, Karaman I, Maier HJ (2006) Acta Mater 54:5477
10. Kocks UF, Mecking H (2003) Progr Mater Sci 48(3):171
11. Li S, Beyerlein IJ, Necker CT, Alexander DJ, Bourke MAM (2003) Acta Mater 52:4859
12. Beyerlein IJ, Li S, Necker CT, Alexander DJ, Tomé CN (2005) Phil Mag 85(13):1359

13. Miyamoto H, Erb U, Koyama T, Mimaki T, Vinogradov A, Hashimoto S (2004) Phil Mag Lett 84:235
14. McNelley TR, Swisher DL (2004) In: Zhu YT et al (eds) Ultrafine grained materials III. TMS, Warrendale, PA, pp 89–94
15. Wu PC, Chang CP, Kao PW (2004) Mater Sci Engng A 374:196
16. Huang X, Borrego A, Pantleon W (2001) Materials Science and Engineering A 319–321:237
17. Dalla Torre FHD, Lapovok R, Sandlin J, Thomson PF, Davies CHJ, Pereloma EV (2004) Acta Mater 52:4819
18. Beyerlein IJ, Tomé CN (2007) Int J Plasticity (in press)
19. Bauccio M (ed) (1993) ASM Metals Reference Book, 3rd ed., ASM International, Materials Park, OH, p 143
20. Chinh NQ, Illy J, Kovacs Z, Horita Z, Langdon TG (2002) Mater Sci Forum 396–402:1007
21. Poortmans S, Verlinden B (2006) Mater Sci Forum 503–504:847
22. Dalla Torre FHD, Pereloma EV, Davies CHJ (2006) Acta Mater 54:1135
23. Han SZ, Lim C, Kim C, Kim S (2005) Metall Mater Trans 36:467
24. Shih MH, Yu CY, Kao PW, Chang CP (2001) Scripta Mater 45:793
25. Rauch EF (1992) Solid State Phenom 23/24:317
26. Stout MG, Rollett AD (1990) Metall Trans 21A:3201
27. Vincze G, Rauch EF, Gracio JJ, Barlat F, Lopes AB (2005) Acta Mater 53:1005
28. Christodoulou N, Woo OT, MacEwen SR (1986) Acta Metall 34(8):1553
29. Li S, Beyerlein IJ, Alexander DJ (2005) Scripta Mater 52:1099
30. Komura S, Horita Z, Nemoto M, Langdon TG (1999) J Mater Res 14(10):4044
31. Beyerlein IJ, Toth LS, In: Zehetbauer, Zhu (eds) Texture evolution in ECAE, Bulk nanostructured materials, (2006) Wiley-VCH, Germany (In press)
32. Davenport SB, Higginson RL, Sellars CM (1999) Philos Trans R Soc of Lon A 357:1645
33. Yu CY, Sun PL, Kao PW, Chang CP (2005) Scripta Mater 52:359
34. Langdon TG (2006) J Mater Sci 41(3):597
35. Peeters B, Seefeldt M, Teodosiu C, Kalidindi SR, Van Houtte P, Aernoudt E (2001) Acta Mater 49:1607
36. Bay B, Hansen N, Hughes DA, Kuhlmann-Wilsdorf D (1992) Acta Metall Mater 40:205
37. Teodosiu C (1996) RIKEN Rev Focus Comput Sci Engng 14:35
38. Cetlin PR, Corrêa ECS, Aguilar MTP (2003) Metall Mater Trans A 35:589
39. Mahesh S, Tomé CN, McCabe RJ, Kaschner GC, Beyerlein IJ, Misra A (2004) Metall Mater Trans A 35:3763
40. Beyerlein IJ, Tomé CN (2006) In: Zhu YT, Langdon TG, Horita Z, Zehetbauer MJ, Semiatin SL, Lowe TC (eds) Ultrafine grained materials IV. TMS, The Minerals, Metals & Materials Society, pp 63–71
41. Hasegawa T, Yakou T, Karashima S (1976) Mater Sci Engng 20:267
42. Wilson DV, Zandrahimi M, Roberts WT (1990) Acta Metall Mater 38:215
43. Han BQ, Lavernia EJ, Mohamed FA (2003) Metall Mater Trans 34A:71
44. Lebensohn RA, Tomé CN (1993) Acta Metall Mater 41:2611
45. Tomé CN, Lebensohn RA (2004) In: Raabe D, Roters F, Barlat F, Chen LQ (eds) Continuum scale simulation of engineering materials: fundamentals, microstructures, process applications. Wiley-VCH Verlag GmbH & Co KGaA, Weinheim, pp 473–499
46. Kocks UF, Tomé CN, Wenk H-R (1998) Texture and anisotropy. Cambridge University Press
47. Tomé CN, Canova GR, Kocks UF, Christodoulou N, Jonas JJ (1984) Acta Metall 32(10):1637
48. Beyerlein IJ, Tomé CN (2006) Mater Sci Engng Technol 36(10):541
49. Xue Q, Beyerlein IJ, Alexander DJ (2006) Acta Mater (in press)
50. Hosford WF (1993) The mechanics of crystals and textured polycrystals. Oxford Univ Press, New York, p 29
51. Phillips Jr WL (1962) Trans Metal Soc AIME 22:845–850
52. Phillips Jr WL, Robertson WD (1958) Trans Metal Soc AIME: 406–412
53. Wu TY, Bassani JL, Laird C (1991) Proc Math Phys Sci 435:1
54. Madec R, Devincre B, Kubin LP (2002) Phys Rev Lett 89:255508-(1–4)
55. Wilson DV, Bate PS (1986) Acta Metall 34(6):1107
56. Tomé CN, Lebensohn RA, Necker CT (2002) Metall Mater Trans A 33:2635
57. Li S, Beyerlein IJ, Alexander DJ, Vogel SC (2005) Acta Mater 53:2111
58. Vogel SC, Beyerlein IJ, Bourke MAM, Tome CN, Rangaswamy P, Xu C, Langdon TG (2002) Mater Sci Forum 408–412:673
59. Li S, Bourke MAM, Beyerlein IJ, Alexander DJ, Clausen B (2004) Mater Sci Engng A 382/1–2:217
60. Budilov IN, Alexandrov IV, Lukaschuk YV, Beyerlein IJ, Zhernakov VS (2004) In: Zhu YT et al (eds) Ultrafine grained materials III. TMS, Warrendale PA, pp 193–198
61. Beyerlein IJ, Tomé CN (2004) Mater Sci Engng A 380:171
62. Nazarov AA, Enikeev NA, Romanov AE, Orlova TS, Alexandrov IV, Beyerlein IJ, Valiev RZ (2006) Acta Mater 54:985
63. Mahesh S, Beyerlein IJ, Tomé CN (2005) Scripta Mater 53:965
64. Estrin Y, Toth LS, Brechet Y, Kim HS (2006) Mater Sci Forum 503–504:675
65. Corrêa ECS, Aguilar MTP, Cetlin PR (2002) J Mater Process Technol 124:384
66. Beyerlein IJ, Tomé CN (2007) Proceedings of THERMEC 2006, Materials Science Forum, vol.539–543, Trans Tech Publications, Vancouver, Canada, July 3–7, pp 3383–3388